Squeezing Visible Light Waves into a 3-nm-Thick and 55-nm-Long Plasmon Cavity

Hideki T. Miyazaki*

*Materials Engineering Laboratory, National Institute for Materials Science,
1-2-1 Sengen, Tsukuba, Ibaraki 305-0047, Japan*

Yoichi Kurokawa

International Center for Young Scientists, National Institute for Materials Science, 1-1 Namiki, Tsukuba, Ibaraki 305-0044, Japan
(Received 30 August 2005; published 7 March 2006)

We demonstrate controlled squeezing of visible light waves into nanometer-sized optical cavities. The light is perpendicularly confined in a few-nanometer-thick SiO_2 film sandwiched between Au claddings in the form of surface plasmon polaritons and exhibits Fabry-Perot resonances in a longitudinal direction. As the thickness of the dielectric core is reduced, the plasmon wavelength becomes shorter; then a smaller cavity is realized. A dispersion relation down to a surface plasmon wavelength of 51 nm for a red light, which is less than 8% of the free-space wavelength, was experimentally observed. Any obvious breakdowns of the macroscopic electromagnetics based on continuous dielectric media were not disclosed for 3-nm-thick cores.

Surface plasmons, electromagnetic surface waves coupled to free electron plasma in metals [1,2], are nowadays familiar to us in biomolecule detection. Since the discovery of the single-molecule sensitivity of Raman scattering at the contact point of silver nanoparticles [3], plasmon resonance at small gaps in metallic subwavelength structures has attracted attention in terms of enhanced spectroscopy. Various geometries have been extensively studied both theoretically [4,5] and experimentally [6–10]. However, the vital problem of reproducible fabrication of nanometer-sized gaps has been left unsolved. In this Letter, we propose a clear-cut architecture of plasmon cavity resonators, in which a nanometer-thick dielectric film is employed as the gap. The spatial extent of the energy can be reduced perpendicularly by metal claddings [11] and longitudinally by large wave vectors of the supported plasmons [12]. We demonstrate the resonant confinement of visible light waves in a dielectric core as thin as 3.3 nm and as short as 55 nm. The minimum wavelength of the plasmon polariton observed is 51 nm for a red light, which is less than 8% of the free-space wavelength. A soft x-ray wavelength for a visible frequency is almost within our reach [13].

The structure of our resonator is simple; it is a so-called MIM (metal-insulator-metal) waveguide with a finite length. Consider a dielectric sheet with a thickness of T between two noble metal slabs. Here we restrict our discussion to $Au/SiO_2/Au$ systems. Figure 1 depicts the analytical dispersion curves [14] of propagating TM (transverse magnetic) modes for various T values. When two insulator-metal interfaces are brought closer to each other, the dispersion curve of a single interface splits into high- and low-energy modes. Figure 1 shows only the low-energy ones for simplicity. Surface plasmons can be excited from a free space without momentum matching simply by perpendicular incidence to the end face [15].

However, due to the matching of the field symmetry, only the low-energy mode is excited. Here we utilize this mode.

When $T = 100$ nm, the dispersion is not so different from that of a single interface. However, when T is reduced, the interaction of two interfaces gets stronger and the dispersion curve of the lower mode becomes flat. Particularly, for T values less than 10 nm, we can obtain plasmons with small wavelengths (λ_p) on the order of 10 nm, i.e., extreme ultraviolet wavelengths, for free-space wavelengths (λ) ranging from visible to near-infrared; they
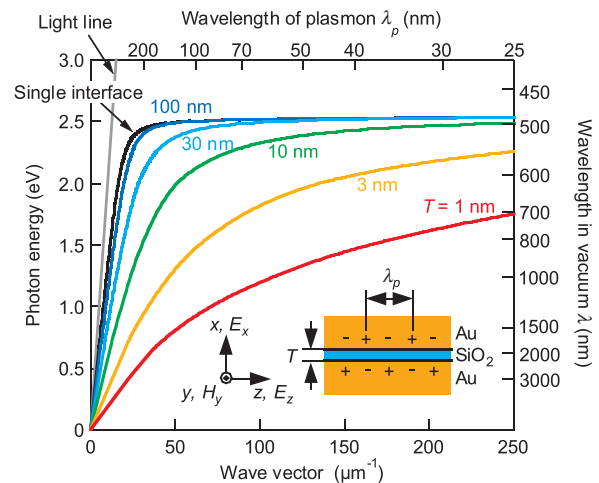

FIG. 1 (color).   Dispersion relations of MIM waveguides for TM modes propagating in the z direction. The geometry, the coordinate system, and the field components of the TM mode are illustrated in the inset. The black solid curve shows the dispersion for a single interface, and colored ones those for low-energy modes for various T values. We used the value of 2.1 and the reported values [27] for the dielectric constants of SiO_2 and Au, respectively.

open a route to nanocavities. Moreover, small T values lead to higher amplitude of excited fields [5]. This can also be understood from the viewpoint of the plasmon density of states inversely proportional to the slope of the dispersion curves [16]. While reproducible realization of gaps narrower than 10 nm by current lithography-based technologies is difficult [9], deposition of nanometer-thick thin film is sufficiently feasible with conventional techniques.

In the course of the investigation on the extraordinary transmission through nanohole arrays [17], Fabry-Perot resonance in narrow slits has been unveiled [18–21]. The plasmon modes supported by the slits are reflected by the end faces, so that the electric field becomes the maximum at the ends, and can form standing waves between two surfaces. In other words, a MIM waveguide with a finite length (L) works as a resonator [19]. Our original point is to realize this slit by depositing a dielectric thin film. Since the nanometer-thick dielectric sheet functions as a cavity resonator for plasmons, we would like to call such a structure *a nanosheet plasmon cavity.*
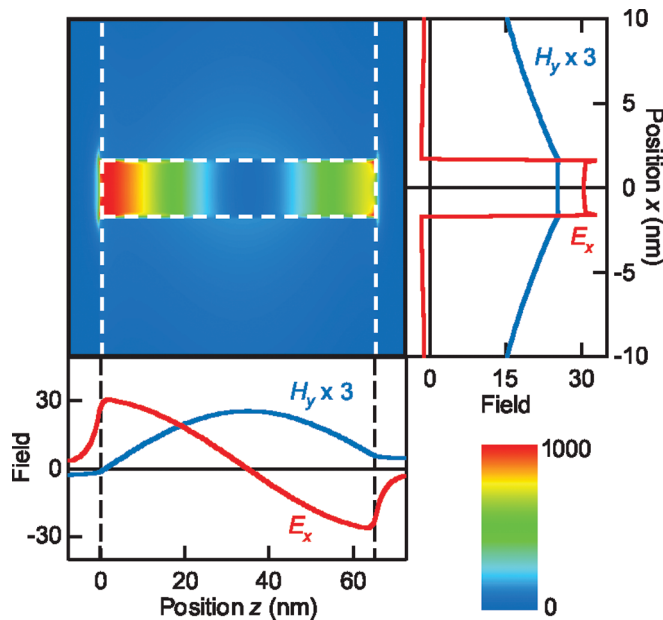

FIG. 2 (color).   Energy density distribution in a MIM waveguide with a finite length. The first-order resonance for $T = 3.3$ nm and $L = 65$ nm. The thickness of the Au slabs in the x direction is 150 nm. A TM (x)-polarized plane wave of $\lambda = 970$ nm is incident from the left. The dashed lines are the borders between Au, SiO$_2$, and free space. Right: Electric and magnetic fields at $z = 2$ nm and $L/2$, respectively. These are typical profiles of the MIM guided mode. Below: Fields at $x = 0$. The electric field shows the maximum amplitudes near both end faces, and the magnetic field exhibits a peak at the center; a typical standing wave of $m = 1$. The fields are the snapshots at the moment of the maximum amplitude. The energy density and the fields are normalized by those of the incident wave. The energy was calculated taking account of the frequency dispersion of the dielectric constant of Au [16,28]. Each corner of the model has a radius of 0.25 nm to avoid unphysically singular values.

Figure 2 shows the theoretical results of the energy density distribution in a cavity at a typical first-order resonance (order number: $m = 1$). In this Letter, we used the two-dimensional (2D) boundary element method [22] for calculation. Perpendicular (x) and longitudinal (z) energy confinement is clearly visualized. Furthermore, the field distribution suggests that the simple standing wave picture inside a MIM waveguide is surely applicable. Note that the electric field is maximized near the entrance and the exit surfaces ($z = 0$ and L). Consequently, we can expose molecules approximately to the maximum field by just letting the molecules adsorbed on the end face of the SiO$_2$ sheet. This is a novel feature, which was not present in conventional optical cavities, and is especially important for the application to enhanced Raman spectroscopy.

MIM geometries have not attracted attention as transmission lines due to their limited propagation lengths [11]: The imaginary part of the dielectric constant of the metal induces Joule heating losses. Nonetheless, giant Raman enhancements were demonstrated in dimers of silver nanoparticles [3], which can be regarded as MIM configurations. From this fact, we expect that the profit from the strong energy confinement of MIM cavities can outweigh the disadvantage of losses.

To fabricate the cavities, Au/SiO$_2$/Au multilayers were first deposited on fused silica substrates by magnetron sputtering. The thickness of the Au layers was fixed to 150 nm and those of the SiO$_2$ film were $T = 56$, 14, and 3.3 nm. Transmission electron microscopy was employed to measure T and to inspect the morphology of SiO$_2$ layers. The result is exemplified in the inset in Fig. 3. Next the Au/SiO$_2$/Au multilayers were processed with a focused
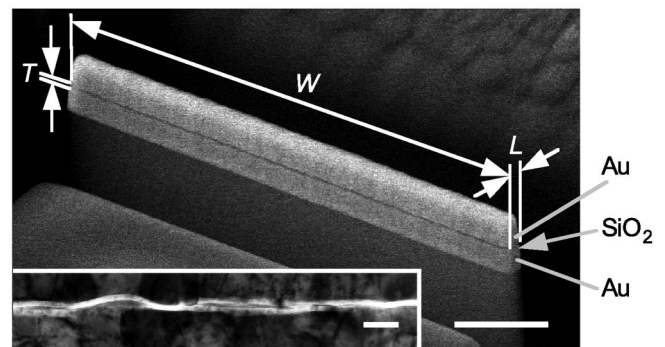

FIG. 3.   Scanning electron micrograph of a fabricated nanosheet plasmon cavity. $T = 14$ nm, $L = 107$ nm, and $W = 3$ μm. Scale bar, 500 nm. Inset: The transmission electron micrograph of the cross section for $T = 3.3$ nm. Scale bar, 20 nm. Although the SiO$_2$ film is wavy due to the surface roughness of the first Au layer, this feature had no influence on the optical properties in this study. The SiO$_2$ film looks duplicated because the microscope specimen has a finite thickness and the vicinities of convex and concave points of the film look brighter.

ion beam from the normal direction, so that rectangular cavities with widths of W and lengths of L are left unmilled as shown in Fig. 3. For each T value, about 20–30 cavities with different L values ($L = 55$–483 nm) were arrayed along one of the edges of the substrate. The structures are assumed to be infinitely long in the y direction in Figs. 1 and 2. To minimize the discrepancy of the experimental samples from the theoretical models, W was set to 3 μm, which is sufficiently long compared with λ_p.

Resonance in a nanostructure can be probed with far-field signals in most cases [4–9]. In this study, the entrance surfaces of the cavities were vertically illuminated with a nearly collimated white light, and the backscattering spectrum only from a selected area around the center of each single cavity was measured, as depicted in Fig. 4(b). The measured quantity is hereafter simply called reflectance. Representative results are displayed in Fig. 4(a). Dips were observed in the reflection spectra for TM polarization, and they systematically shifted as a function of L. Calculated results of the reflectance and the field enhancement at the center of the entrance surface are compared in Fig. 4(c). It is obvious that the reflection dips are the signs of the resonances. At the peaks of the field enhancement
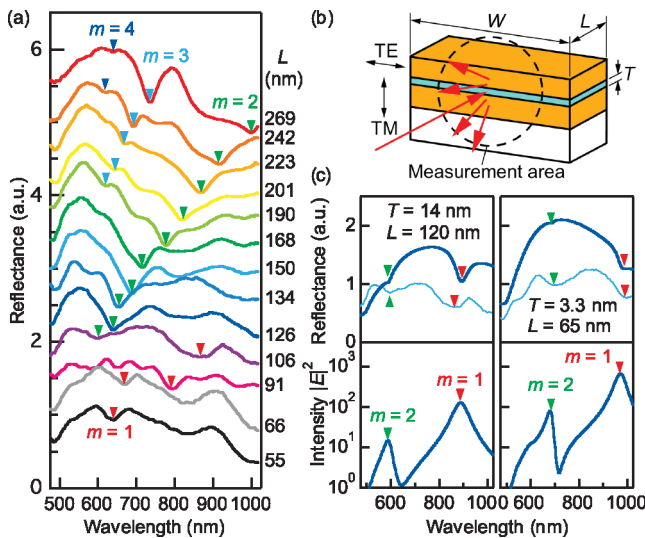
spectra, standing waves as exemplified in Fig. 2 were confirmed by the calculation of the field distributions. In addition, Fig. 4(c) manifests the agreement of the dip positions in the experimental reflection spectra with those by the calculation. By comparison with the calculation, the major dips in Fig. 4(a) were assigned to the resonances of $m = 1$–4. Similar results were obtained also for $T = 56$ and 3.3 nm. In contrast, remarkable features were not found in the reflection for TE (transverse electric) polarization. Thus, the Fabry-Perot resonance of plasmon polaritons in the fabricated cavities was successfully demonstrated. Several minor dips discernible in the spectra for small L values in Fig. 4(a) were not reproduced by the calculation. These could be due to the transverse modes in the y direction.

At the mth resonance in a cavity with a length of L, the corresponding wave vector of the propagating plasmon, k, is expressed as $k = 2\pi/\lambda_p = m\pi/L$. Therefore, the dispersion relations of the plasmon in the cavities can be experimentally determined [23]. In Fig. 5, the reflection dips observed were plotted. The resonances of various orders for various L values formed single dispersion curves unique to each T value. Furthermore, the experimental results showed fairly good agreement with the analytical dispersion curves [14] of MIM waveguides. This also proves that the macroscopic electromagnetics, in which the spatial dispersion effects [24] are neglected, is applicable to a 3-nm-thick core so far as far-field responses are discussed. Nanometric slits can be regarded as media with a large refractive index n [19]. The dashed lines in Fig. 5 indicate the dispersions for representative n values. A red light of $\lambda = 651$ nm in vacuum is confined in the cavity as

FIG. 4 (color). (a) Measured reflectance for various L values. $T = 14$ nm and TM polarization. The individual spectra are offset by 0.04 from one another for visibility. Arrows indicate the major dips. (b) Schematic drawing illustrating the incident, the collected scattered light, and the measurement area (diameter: 2 μm). (c) Calculated reflectance (upper) and intensity enhancement at the center of the entrance surface (lower) for TM polarization for representative T and L values. The field is normalized by that of the incident light. The thin lines indicate the experimental reflection spectra for similar parameters (left: $L = 106$ nm; right: 61 nm). The reflection dips and the field peaks are denoted by arrows. The fields in Fig. 2 correspond to the $m = 1$ peak in the right panel. The Q values of the resonances are 10–20.
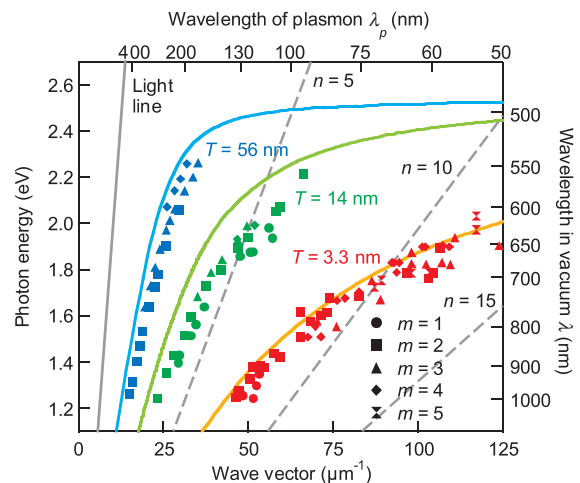

FIG. 5 (color). Experimentally obtained dispersion relations. Solid curves: Analytical dispersion of MIM waveguides. Dashed lines: Propagation in the media with refractive indices of n drawn for reference. The non-negligible discrepancy between the analytical model and the experiment for $T = 14$ nm probably originates from an error in the thickness measurement.

PHYSICAL REVIEW LETTERS

a surface plasmon polariton with a wavelength of $\lambda_p = 51$ nm. This wavelength is equivalent to that for $n \simeq 13$. Such a large index is unattainable by bulk materials.

Larger wave vectors enable us to realize smaller cavities. The minimum modal volume in this study is $V = 0.000\,95 \ \mu m^3 = 0.0012\lambda^3 = 1.6TLW$ [25]. This value was estimated according to the definition of Foresi *et al.* [26] with a slight modification; we used the maximum energy density on the z axis for the normalization instead of the maximum density in the whole space, because the maximum but singular value at the edge of the Au claddings gives an unrealistically small V value. Despite the large width of $W = 3 \ \mu m$, the estimated modal volume is very small. For cavities of $W \simeq \lambda_p$, further reduction of more than one order is possible. Although the Q value is small, Q/V values comparable to those of the conventional optical resonators might be obtained because of the very small V.

In summary, we proposed the nanosheet plasmon cavity as a new configuration of optical resonators and demonstrated energy confinement in volumes much smaller than the free-space wavelengths ($\simeq 0.001\lambda^3$). Although the estimated intensity enhancements for the fabricated cavities resulted in modest values as high as $|E|^2 \simeq 10^3$ [Fig. 4(c)], a further enhancement should be possible for periodically arrayed cavities by the interaction with the plasmons along the entrance and the exit surfaces [18]. Reduction of the width W would also lead to a larger field enhancement by the energy confinement in a much smaller volume. For a thinner core, a breakdown of the macroscopic electromagnetics is expected; it would probably result in enhanced losses [24] and resultant deterioration in resonances. Wave vector dependence of the dielectric functions should be considered.

*Electronic address: MIYAZAKI.Hideki@nims.go.jp

[1] W. L. Barnes, A. Dereux, and T. W. Ebbesen, Nature (London) **424**, 824 (2003).
[2] J. Pendry, Science **285**, 1687 (1999).
[3] H. Xu, E. J. Bjerneld, M. Käll, and L. Börjesson, Phys. Rev. Lett. **83**, 4357 (1999).
[4] M. Futamata, Y. Maruyama, and M. Ishikawa, J. Phys. Chem. B **107**, 7607 (2003).
[5] E. Hao and G. C. Schatz, J. Chem. Phys. **120**, 357 (2004).
[6] H. Tamaru, H. Kuwata, H. T. Miyazaki, and K. Miyano, Appl. Phys. Lett. **80**, 1826 (2002).
[7] W. Rechberger *et al.*, Opt. Commun. **220**, 137 (2003).
[8] D. P. Fromm *et al.*, Nano Lett. **4**, 957 (2004).
[9] L. Gunnarsson *et al.*, J. Phys. Chem. B **109**, 1079 (2005).
[10] P. Mühlschlegel *et al.*, Science **308**, 1607 (2005).
[11] R. Zia, M. D. Selker, P. B. Catrysse, and M. L. Brongersma, J. Opt. Soc. Am. A **21**, 2442 (2004).
[12] J. Takahara and T. Kobayashi, Opt. Photonics News **15**, No. 10, 54 (2004).
[13] H. A. Atwater *et al.*, MRS Bull. **30**, 385 (2005).
[14] E. N. Economou, Phys. Rev. **182**, 539 (1969).
[15] G. I. Stegeman, R. F. Wallis, and A. A. Maradudin, Opt. Lett. **8**, 386 (1983).
[16] I. Gontijo *et al.*, Phys. Rev. B **60**, 11 564 (1999).
[17] T. W. Ebbesen *et al.*, Nature (London) **391**, 667 (1998).
[18] J. A. Porto, F. J. Garcia-Vidal, and J. B. Pendry, Phys. Rev. Lett. **83**, 2845 (1999).
[19] S. Astilean, Ph. Lalanne, and M. Palamaru, Opt. Commun. **175**, 265 (2000).
[20] H. E. Went *et al.*, Appl. Phys. Lett. **77**, 2789 (2000).
[21] J. Lindberg *et al.*, Opt. Express **12**, 623 (2004).
[22] C. A. Brebbia, J. C. Telles, and L. C. Wrobel, *Boundary Element Techniques* (Springer, Berlin, 1984).
[23] G. Schider *et al.*, Phys. Rev. B **68**, 155427 (2003).
[24] I. A. Larkin, M. I. Stockman, M. Achermann, and V. I. Klimov, Phys. Rev. B **69**, 121403 (2004).
[25] We obtained this volume simply as the product of *the modal area* determined by 2D calculation and W, assuming that the extent of the leaked fields to the free space is negligible against W.
[26] J. S. Foresi *et al.*, Nature (London) **390**, 143 (1997).
[27] P. B. Johnson and R. W. Christy, Phys. Rev. B **6**, 4370 (1972).
[28] L. D. Landau, E. M. Lifshitz, and L. P. Pitaevskii, *Electrodynamics of Continuous Media* (Butterworth-Heinemann, Oxford, 1984), 2nd ed.